

Experimental and numerical investigation of saltwater intrusion dynamics on sloping sandy beach under static seaside boundary condition

Chittaranjan Dalai ^{a,*}, Selva Balaji Munusamy ^{b,c}, Anirban Dhar ^c

^a School of Water Resources, Indian Institute of Technology Kharagpur, West Bengal 721302, India

^b Discipline of Civil Engineering, Indian Institute of Technology Gandhinagar, Gujarat 382355, India

^c Department of Civil Engineering, Indian Institute of Technology Kharagpur, West Bengal 721302, India



ARTICLE INFO

Keywords:

Saltwater intrusion
Circulation pattern
Pore water pressure
Sloping sandy beach

ABSTRACT

Two-dimensional sandbox experiments were conducted to investigate the variable-density circulation and flow patterns in sloping beach configurations. The experiments provide new benchmark results for validating the sandbox models based on quantitative and qualitative measurements. Previous studies have considered density dependent flow in porous media, vertical beach face saltwater boundary, and multilayered hydrogeology ignoring a sloping beach face, which is a much more common phenomenon in real world. The present study considers sloping beach face under both homogeneous and low-permeability strata configurations. The geohydraulic processes encountered were quantified through pore-water pressure measurements and image analysis techniques. Moreover, validations were performed with numerical simulations (FEFLOW). A simple image analysis procedure is proposed with respect to two-dimensional laboratory scale benchmark experiments. Experimental results provided a detailed circulation flow path within and outside the saltwater wedge with sloping beach face. Fingering effect in porous media was also observed for both the experiments during initial time periods. Stability analysis shows the existence of a stationary convective flow pattern followed by gravitational instabilities under the quasi-steady state condition.

Density-dependent groundwater flow is described mathematically by a conservation-of-mass equation together with a density-dependent form of Darcy's Law.

1. Introduction

Variable-density flow in porous media is related to the dynamics of groundwater flow in coastal aquifers. Density driven flow in porous media remains one of the challenging problems owing to its inherent non-linearity, and limited availability of analytical solutions and availability of standard/field data set [1]. In recent years, different in-situ observation based methods were proposed to identify the fluid dynamics of density dependent flows [2–4]. However, experimental quantification is necessary to evaluate the performance of mathematical/numerical models. The laboratory experiments (or benchmark tests) give advantages of known boundary and initial conditions, known porous material properties over the field experiments. Thus laboratory sand box model can be used as a useful instrument for flow visualization and for in-situ measurements. Generally, one-dimensional experiments are performed to study the behavior of flow in porous media under the influence of high density fluid [5–8]. Few studies [9–11] were carried out using laboratory scale two-dimensional (2D) sandbox experiments for identifying interface between two varying density fluids and their flow through stratified porous medium. Laboratory-scale experiments are widely used to investigate the behavior of saltwater interface (SWI) [9–17]. These studies mostly focused

on the dispersive mixing zone while solving the variants of the Henry problem [18]. Recent studies are also available on numerical simulation of density dependent flows [19–22]. Most of the works have either used a vertical saltwater boundary or homogeneous configuration to understand the density dependent flow process.

The density gradient at sloping (non-vertical) boundary plays a vital role in changing the hydraulic gradient and contaminant transport across the SWI. The previous works focused on the position, shape and thickness of the saltwater-freshwater transition zone for density dependent flow in porous media. However, these studies have rarely observed convective saltwater circulation phenomenon [23]. It is well known that variable density flows in porous media can become unstable [24]. The occurrence of fingering is caused by flow instabilities due to differences in viscosity and density values between two miscible fluids. Instabilities and fingering develop when a denser fluid lies above the lighter fluid [25–28]. Viscous fingers develop and can be visualized in the form of the corrugated interface [29]. The fingers propagate rapidly, until they reach a stable convective flow regime.

The results of density-coupled groundwater flow simulations are typically represented as isolines [30–32] or vector plots of the groundwater velocity [33,34]. Experimentally saltwater circulation pattern

* Corresponding author.

E-mail address: cdchittaranjan1@gmail.com (C. Dalai).

cannot be determined from these types of information. Circulation patterns in steady state mixed convection problems can be identified from the streamline plots. The density-driven circulation can be conceptually divided into two consecutive processes: (i) flow of high density fluid (in counter clockwise direction) towards low density fluid due to density gradient, and (ii) upward flow of low density fluid towards free surface of the interface. Moreover, limited numbers of studies are available on growth of circulation pattern due to density driven forces [23].

The steady state interface of freshwater/saltwater was studied by many researchers in the context of multiple permeable layers. Limited number of studies are available on the effects of low permeability layer on SWI [35–37]. However, none of these studies have reported understanding of the density dependent flow process associated with thin stratified low permeability layer. The relative position and thickness of the stratified porous layer has significant effect on the density dependent flows. As per our knowledge, no study has presented laboratory experiments to study quantitative and qualitative saltwater dynamics in porous media. The present study provides the pore water pressure variation under sloping beach face condition for the experimental time periods. This quantitative analysis captures the dynamics of flow and transport processes. Variable density flow experiment is an essential tool to test the reliability of numerical simulations under realistic geometric conditions. [10] has performed laboratory scale experiment to get benchmark data for density dependent Henry problem.

The present study extends the experimental analysis to both confined and unconfined strata configurations. The aim of this study is to provide reliable data for validation of numerical simulation. The present work also focuses on effect of low permeability layer on SWI through laboratory experiments and numerical studies. Evolution of time dependent interface was captured through experiments. Moreover, flow circulation patterns were investigated in different zones (saltwater/freshwater). Experimental data were acquired in the forms of images and pore water pressure measurements (through pressure transducers). Interface movement and flow circulation patterns were determined based on processed images. These results were validated by using a numerical simulation model FEFLOW [38].

2. Methodology

The overall work can be divided into three parts (i) experimental investigation (ii) image processing, and (iii) numerical simulation. Individual components (Figure S1) are described in the following sub-sections.

2.1. Experimental setup

Experimental investigation was carried out with a two-dimensional Sandbox Model setup (Fig. 1)(3.1 m length × 1.0 m height × 0.020 m wide) to model the density dependent flow and transport through porous media. The sandbox is composed of standard stainless steel exterior frame and two transparent glass plates (80 mm thick). The two plates are parallelly placed to each other with a separation distance of 0.020 m. The internal width is kept very small to ensure two-dimensional flow in vertical and longitudinal directions. Two water reservoirs (each 50 mm length) are available at both ends. The right reservoir (Zone C) is used to feed (flux condition) freshwater flow to the system. Constant head condition is maintained with left reservoir (Zone A, filled with saltwater) and overflow outlet pipe (5 mm diameter) place at a height of 0.64 m from the base of the model. Stainless steel mesh (0.1 mm opening) is used to separate both the reservoirs from the middle sand box zone (Zone B). The top of the setup is in direct contact with the atmosphere representing unconfined aquifer condition. Bottom part of the setup has 18 flow controlling outlets including one each at the bottom of the end reservoirs (Zone A and Zone C). The back side of glass wall has 59 openings (8 mm diameter) for taking pressure measurements and injection-extraction of fluid. In the present study, six

pressure transducers (STJE from Honeywell; PS1 to PS6) were placed in a horizontal line 0.57 m above the floor. To prevent entry of porous material, screens were used at the connection points between flexible pipes (to connect the pressure transducer and setup) and openings at back side glass wall.

The Zone B was packed with commercially available coarse sands to represent illustrative unconfined coastal aquifer material followed by a sloping beach surface (slope ≈ 15°). The clean sand was relatively uniform with $d_{50} = 1.02$ mm and $d_{60}/d_{10} = 1.4$. A wet packing method similar to [39] was used to obtain uniform sand packing with minimum entrapped air to satisfy homogeneous isotropic condition. Clean sand was placed in 15 layers of similar thickness. Each layer was carefully tamped down. The average hydraulic conductivity value was subsequently derived using Darcy's law as given in [40]. However, the explicit measurement of hydraulic conductivities in different coordinate directions is a challenging task. The uniform, homogeneous, isotropic hydraulic conductivity value was determined from the numerical model calibration process. The average hydraulic conductivity value of the saturated material was estimated as 420 m/d. Average porosity value of 0.38 was used.

The second configuration with 0.03 m thickness of low permeable layer was considered (Figure S2). The low permeability layer (bentonite clay) was placed at 0.22 m from the bottom boundary as shown in Fig. 1(b)(Figure S3). A thin 0.03 m layer of bentonite clay was maintained throughout the length of porous media.

The water was supplied to the end reservoirs (freshwater to Zone C and saltwater to Zone A). A silastic tube of 7 mm internal diameter was placed into the reservoirs to supply water through peristaltic pump (PP-50vx from Electrolab) at a desired flow rate. Two peristaltic pumps (max flow rate: 250.44 l/d) were utilized for the experimental purpose. Saltwater solution of volume 20 l was prepared prior to the experiments by dissolving commercial salt (NaCl) into freshwater at a concentration of 36.16 g/l to achieve a density of 1025 kg/m³. The density was measured digitally with a CTD Driver [D127 × (D1272 50 m) from Schlumberger] and manually by using mass/volume ratio. To distinguish the saltwater from the freshwater, Rhodamine B type(Lobachemie) tracer with concentration of 0.25 g/l was dissolved with salt to trace the saltwater movement in Zone B. The rhodamine tracer has been used successfully in previous studies [12,41–43]. Batch sorption experiments using UV spectrophotometry (OR3100 UV spectrophotometry ORLAB) were performed by monitoring the absorbance. No measurable sorption of dyes on the clean sand were observed.

Prior to the experiments, freshwater flow from right side was allowed at a constant rate along with freshwater constant head in the left sloping beach part to achieve a zero saltwater intrusion and aquifer material saturation conditions simultaneously. Excess water was drained through the overflow outlet situated in the left side of Zone A. Thus the physical system got stabilized under freshwater flow condition. After initial conditioning of the experimental setup, saltwater was introduced slowly in the Zone A with a constant head of 0.64 m by using peristaltic pump. Excess amount of saltwater was supplied into the left reservoir to ensure flushing of freshwater floating at the surface (above sloping beach face) in Zone B.

A rectangular grid (0.10 m × 0.05 m) was marked on the frontal glass surface of the sand box model. Instantaneous movement of saltwater was visually tracked with the physical grid marked on the glass surface. During image acquisition process points placed at four corners of the Zone B (rectangular in shape) were utilized as static control points. These static control points were used to define the scale and orientation of the all digital images under a unique reference frame. Two Halogen Lights (1000 watt, SUNGUN photographic products) were placed in the front side of the experimental setup to ensure homogeneity of the light throughout the test section (Zone B). A Digital Single-Lens Reflex (DSLR) camera (Nikon d5100) was placed centrally in front of the Sand Box Model at 1 m distance on a fixed tripod. Images were captured at 2 s time interval with the camera. The acquired images were analyzed suitably with an image processing technique.

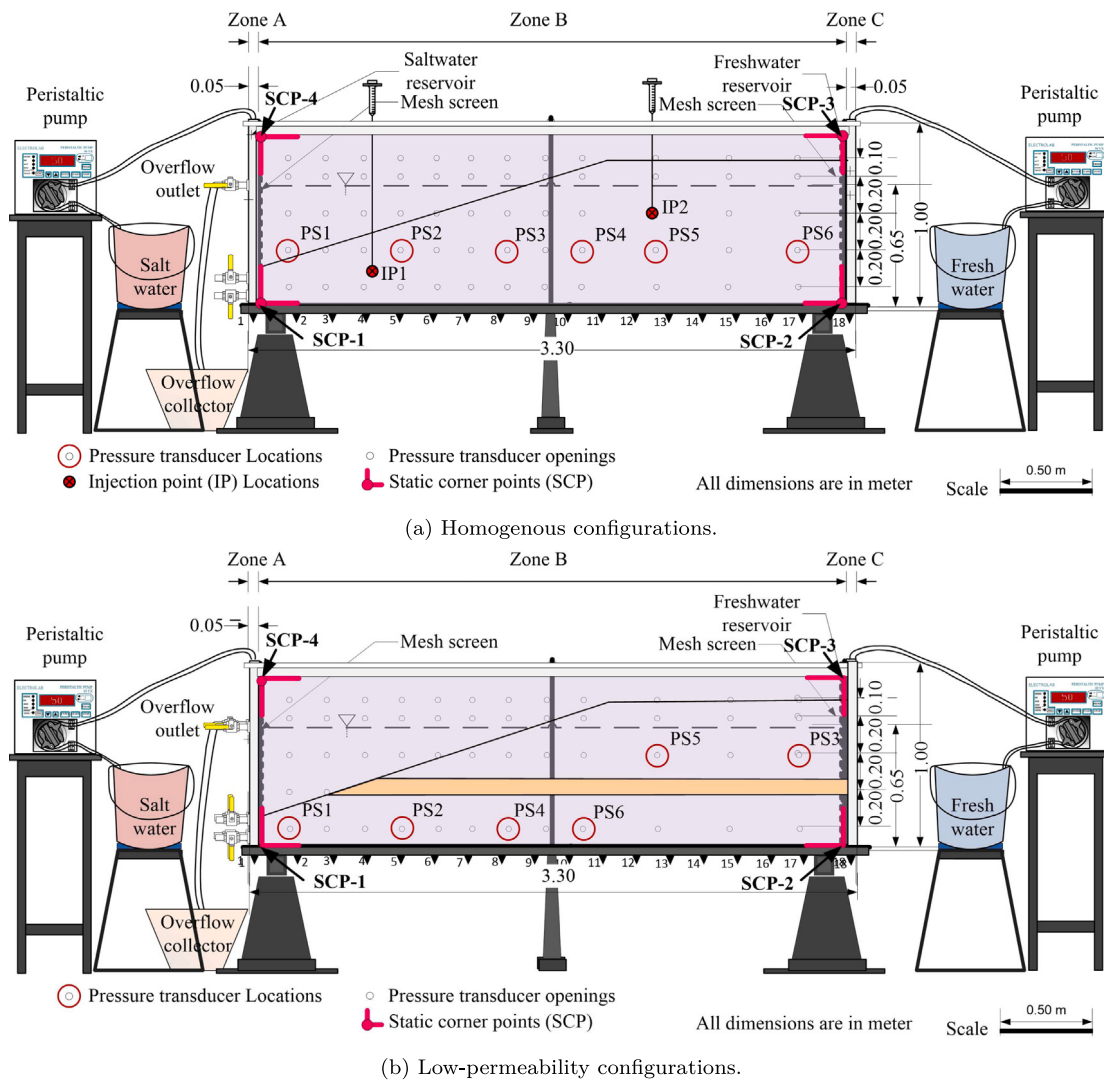


Fig. 1. Schematic diagram of the sandbox model setup.

3. Numerical modeling approach

Consistency of the experimental data was assessed through finite element based numerical simulation in FEFLOW [44]. The constitutive relationship between the hydraulic conductivity, soil saturation and capillary pressure head was prescribed by the van Genuchten model in Richard's equation for modeling of unsaturated-saturated flow. Mathematical details regarding governing equations, boundary conditions and solution method are available in [38]. The laboratory based physical model, corresponding numerical equivalent domain, and relevant boundary conditions are shown in Fig. 2. Top and the bottom boundaries were specified with no flow condition. Freshwater discharge from right boundary was specified as Neumann flux type boundary condition. The hydrostatic pressure boundary condition was specified along sloping boundary (present in Zone B). Initially, the domain was saturated with freshwater at constant flux from the right side (freshwater concentration). An optimal element size of 0.004 m was obtained from mesh convergence study. Meshes with finer and coarser spatial discretizations were tested to establish whether the above element size was adequate to provide numerically converged solutions. The longitudinal and transverse dispersivity values (0.004 m and 0.0004 m) were determined from the calibration process within the range reported in [45]. The hydraulic conductivity value was also determined from the calibration process within the range of clean sand [46]. The molecular

Table 1
Numerical simulation parameters.

| Parameters | Symbols | Value | Unit |
|-------------------------------------|------------|--------------------|------------------------|
| Horizontal length | L | 2.5 | m |
| Domain thickness | H | 1.0 | m |
| Porosity | ϵ | 0.38 | - |
| Saltwater level | h_f | 0.66 | m |
| Freshwater density | ρ_0 | 1000 | kg/m^3 |
| Saltwater density | ρ_s | 1025 | kg/m^3 |
| Saltwater concentration | C_s | 35 | kg/m^3 |
| Longitudinal dispersivity | β_L | 0.004 | m |
| Transverse dispersivity | β_T | 0.0004 | m |
| Molecular diffusion coefficient | D | 1×10^{-9} | m^2/s |
| Density Ratio | α | 0.025 | - |
| Hydraulic conductivity (clean sand) | K_s | 420 | m/d |
| Hydraulic conductivity (bentonite) | K_B | 0.00004 | m/d |

diffusion value of $1 \times 10^{-9} \text{ m}^2 \text{ s}^{-1}$ was used in the numerical simulations. The simulation parameter values are reported in Table 1.

4. Image analysis

In recent times, image analysis has emerged as a proxy measurement technique for physical experiments. A number of studies are available

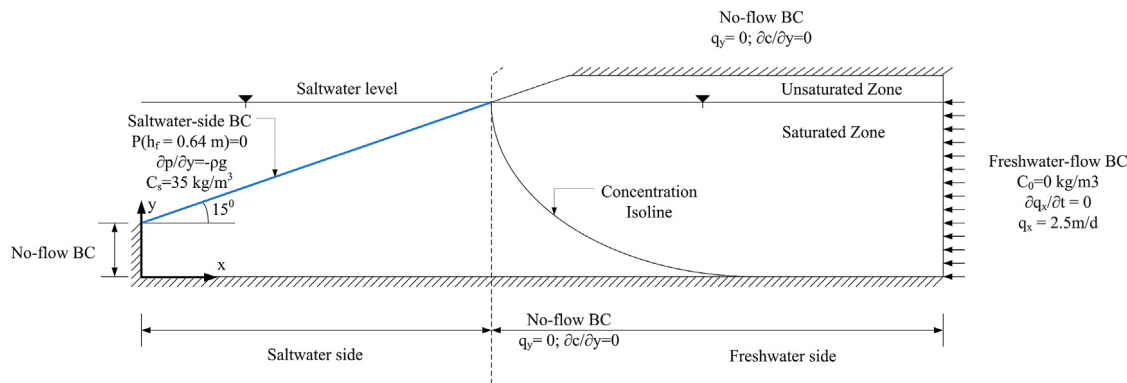


Fig. 2. Boundary conditions for homogeneous configuration for the numerical simulations.

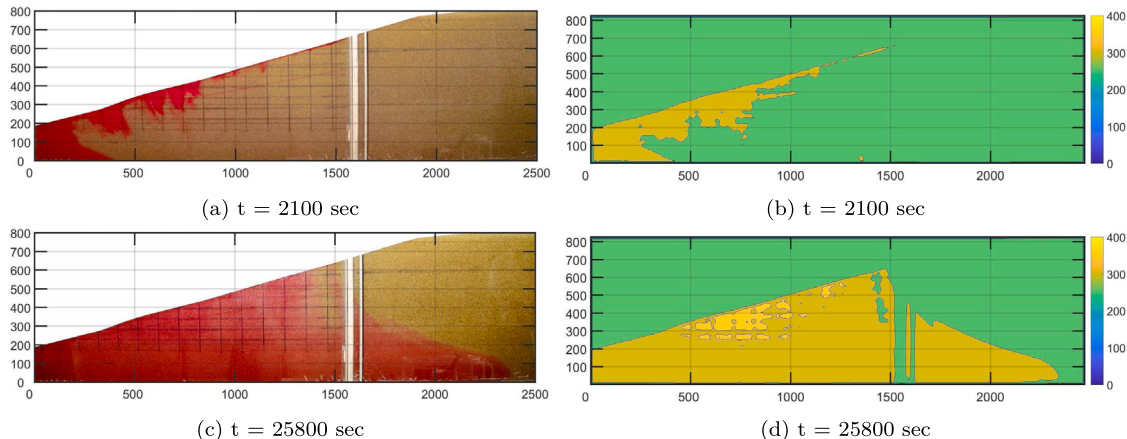


Fig. 3. The laboratory experiment results showing the development of the saltwater configuration with time. Note that both colors and contours represent the salinities of the water. The color map indicates the magnitude of the density water flow. (All dimensions are in mm.) (For interpretation of the references to color in this figure legend, the reader is referred to the web version of this article.)

on image analysis for solute transport [47–52]. However, these techniques are relatively complex in nature. Robinson et al. [53] suggested that light source placed at the back side for tracer experiment with relatively transparent glass beads can provide reasonably good results. The intensity of the light transmitting through highly porous glass beads was uniform. In sand box model light source cannot be placed at the back side due to opaque nature of the material. Thus two Halogen Lights were provided from the front side.

In the present work, a simplified interface identification technique for saltwater intrusion in sandbox is proposed. An image covers the complete area of the sandbox model. Image is a combined representation of number pixels and each pixels store the color information. A color can be regarded as a proportional mixture of red(R), green(G), and blue(B) values [54]. It is convenient to regard a color as vector in a three-dimensional R-G-B color space. In concentration space for a single concentration value there exists multiple combinations of R-G-B. The multiplicity exists due to combined effect of tracer and sand color. Thus specification of a single concentration value for a particular R-G-B cluster will provide misleading information [55].

A mapping between concentration and color space requires an equivalent functional relationship. After preliminary analysis on test section (Fig. 1b), it was observed that out of three basic colors (R-G-B) blue (B) is always dominant. Interface movement identification was heavily influenced by the difference in red (R) and green (G) colors. Thus pixel level modification was performed to obtain a concentration equivalent single value. The simplified expression can be written as

$$\bar{C}_{i,j} = 255 + [D_{i,j}^R - D_{i,j}^G] \quad (1)$$

where $\bar{C}_{i,j}$ is converted pixel value applied to original image at pixel location i, j of image matrix. $D_{i,j}^R$ and $D_{i,j}^G$ are the digital number (DN) values for red and green colors at pixel location (i, j) , respectively.

The image analysis provides information about the interface movement over time. Total 820 images were acquired at a 2 s time interval for Zone B. The raw images were aligned and corrected with respect to the static control points. The cropped images corresponding to the test section (Figure S3) were utilized for next level of analysis. These images provide scattered/noisy information about the color distribution. Thus neighborhood averaged images were used for further analysis. Resulting images provided usable tracer movement information for numerical analysis. Interface was assumed corresponding to 0.5 isochlor. A similar porous material (same material characteristics) was utilized for both homogeneous and low-permeability layer configuration experiments (see Fig. 4).

5. Results and discussion

The density in the saltwater reservoir was continuously monitored using a CTD Driver (Fig. 5(a)). The measurements for density dependent flow experiments were taken only after stabilization of the density measurements. Fig. 5 shows the starting point (after density stabilization) of the both experiments ($t=0$).

Information regarding interface variation over vertical cross-section was extracted from the experimental images. The processed images (Fig. 3 and Fig. 4) provide the spatial distribution of tracer concentration at various times. The results reveal that the concentration distribution evolves slowly over time. The interface movement was

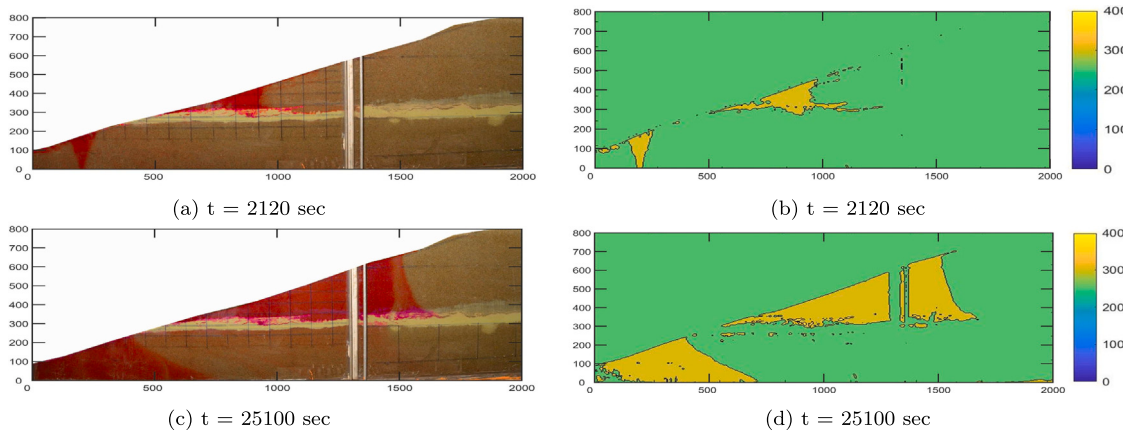


Fig. 4. The laboratory experiment results showing the development of the saltwater configuration in low-permeability strata. Note that both colors and contours represent the salinities of the water. The color map indicates the magnitude of the density water flow. (All dimensions are in mm.) (For interpretation of the references to color in this figure legend, the reader is referred to the web version of this article.)

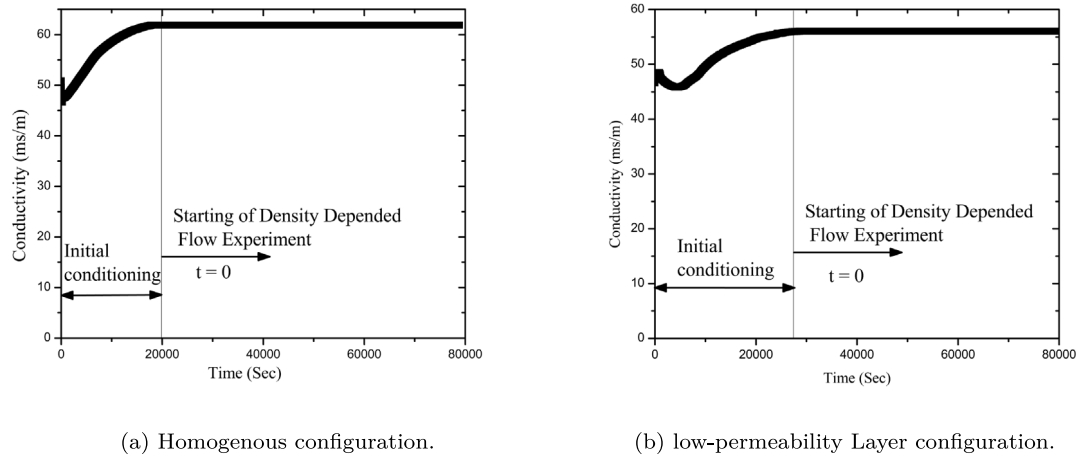


Fig. 5. Observed conductivity profile at saltwater side.

better captured through the processed images compared to experimental ones due to the representation in terms of the converted pixel value. These processed interface movement information were utilized for calibrating and validating by numerical simulation results.

Fig. 6 provides the comparison of processed images and numerical simulation results at different time periods. The combined figures (Fig. 6) clearly show that the interface movements were captured quite reasonably by the numerical simulation model. However, the numerical simulation model was failed to capture the local fingering effect visible in the experimental results. It is a limitation of the numerical conceptualization through Richard's equation simulation model. The finger effect can be captured with a more complex model.

The numerical simulation results over-predicted the interface movement in vertical direction. This is due to the fact that convective instabilities occur during the travel of a heavier fluid (saline water) in presence of a lighter fluid (fresh water) flow and under the perturbations of the natural medium [29].

Experiment was conducted with stratified layers. Fig. 7 indicates that the thickness of low-permeability layer has a significant impact on saltwater front movement. The saltwater movement was separated by the thickness of low permeability layer. The upper portion of the low permeability layer represented as unconfined zone. Similarly, the lower portion represented as confined zone. In confined zone SWI movement was small compared to the upper portion due to difference in freshwater movement. Numerically the saltwater front movement

was better captured in stratified case compared to single layer configuration. Nevertheless, differences exist between the experimental and simulated results.

5.1. Saltwater circulation under quasi-steady state condition

The saltwater circulation study was conducted before attaining the quasi-steady state condition in terms of movement of the location. The external tracer was injected through the location *IP1* 1 inside the saltwater wedge. A total 60 ml Fluorescein Sodium (Loba chemie) liquid solution was injected (Fig. 1(a)) at *IP1* (600 mm, 180 mm) with 2.1 g *NaCl* to maintain a density of 1025 kg/m³ within the saltwater wedge. The tracer plume movement was captured through photographs (Fig. 8) taken at an interval of 2 s. These visual images revealed the saltwater circulation pattern within the saltwater wedge for sloping beach portion in terms of tracer movement. Density difference between fluids produces convective flows. Moreover, freshwater flux towards saltwater creates a density gradient along the diffused interface. The gradient of density introduces gravitational instabilities which in turn facilitates circular pattern within the system. The tracer dye follows the circulating fluid flow path (Fig. 8).

5.2. Freshwater flow patterns under quasi-steady state condition

Tracer was also injected at a uniform rate in the freshwater zone (Fig. 1(a)) at location *IP2* (2140 mm, 480 mm) to identify the flow

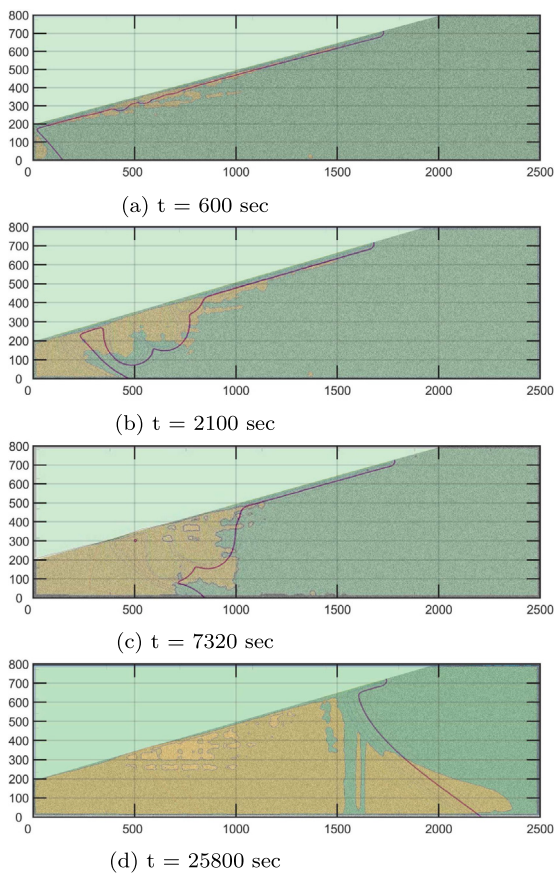


Fig. 6. The results of Homogeneous configurations show development of the SWI with time (t' — the initial stages to t — the final stages), it represents the overlap of both the results between the laboratory experiment (spatial dye distribution) and the computed salinity contours from the numerical simulations for better comparative study.

pattern. A total 30 ml Fluorescein Sodium (Loba chemie) liquid solution was injected (Fig. 1(a)). Absorption rate in coarse sand is minimal for this tracer [56]. A uniform interval of 2 s was used for capturing photographs (Fig. 9) of tracer movement. Starting from initial injection the tracer movement was recorded till it reached on the top of the saltwater surface just attached to the sloping beach portion. It is evident that fresh water particles move along the interface zone and rise up due to density difference between the saline and fresh waters.

5.3. Numerical validation

Information regarding tracer movement over the vertical cross section was extracted from the experimental images. Processed images (Fig. 3) provide the spatial distribution of tracer concentrations at various times. The results reveal that the tracer distribution evolves slowly over time. The tracer movement was better captured through the processed images compared to experimental ones due to the representation in terms of the converted pixel values. These processed interface movement information were utilized for calibrating and validating the numerical simulation results. The numerical simulation results for injection through IP1 and IP2 experimental are presented in Fig. 8 and Fig. 9. Time evolution of injected tracer was captured through numerical simulation. It is evident that the simulated tracer movement matches with the experimental pattern. However, small discrepancies are present due to difference in dispersivity value.

Figs. 10 and 11 represent Darcy's flux, which relates the fluid density and pressure gradients to the discharge vector at a point. Velocity vectors are visible for both the homogeneous 10 and low permeable

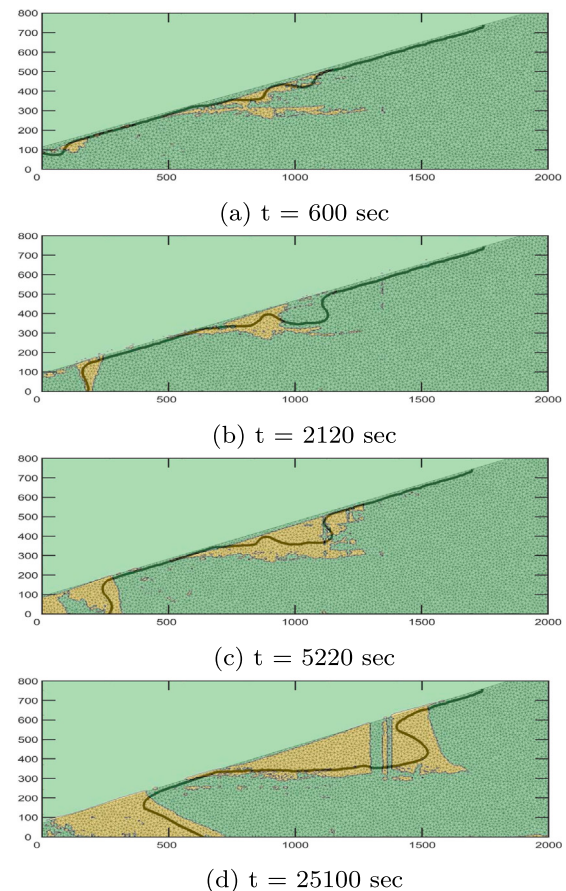


Fig. 7. The results of low-permeability strata configuration show development of the SWI with time (t' — the initial stages to t — the final stages). its represents the overlap of both the results between the laboratory experiment (spatial dye distribution) and the computed salinity contours from the numerical simulations for better comparative study.

layer 11 configurations. In the both configurations the flow is mainly towards the saltwater region. This increases pressure towards the freshwater zone. In the closer region near to seepage face portion, the main flow (freshwater flow) is in the opposite direction (i.e., towards free surface). Flow vectors show that the saltwater approximates the wedge and converges with freshwater. The conflict of these vectors creates the dispersion zone. The motion vectors associated with a smoothly moving solute particle in a steady state field.

5.4. Pore water pressure measurement

Front tracking is the most complex part of density dependent flow problems. In general, the density of a fluid is influenced by temperature (density decreases when temperature increases) and pressure (density increases when pressure increases due to compressibility). Experimental determination of the volume-averaged velocity would appear to be extremely difficult. Direct measurement of hydraulic head is not practically feasible for non-hydrostatic, unsteady variation within porous media. However, measurement of the point pore water pressure is feasible experimentally. Thus, the pore water pressure measurements are used as latent variable for hydraulic head. The data sampling at higher range to remove the biasness from the collected pore water pressure data. The pressure data provides high quality information for density-driven flow in porous media [57]. The pressure transducers were directly connected to the openings in the glass wall through flexible tube (8 mm diameter). Data were collected at 20 Hz frequency from all the pressure probes.

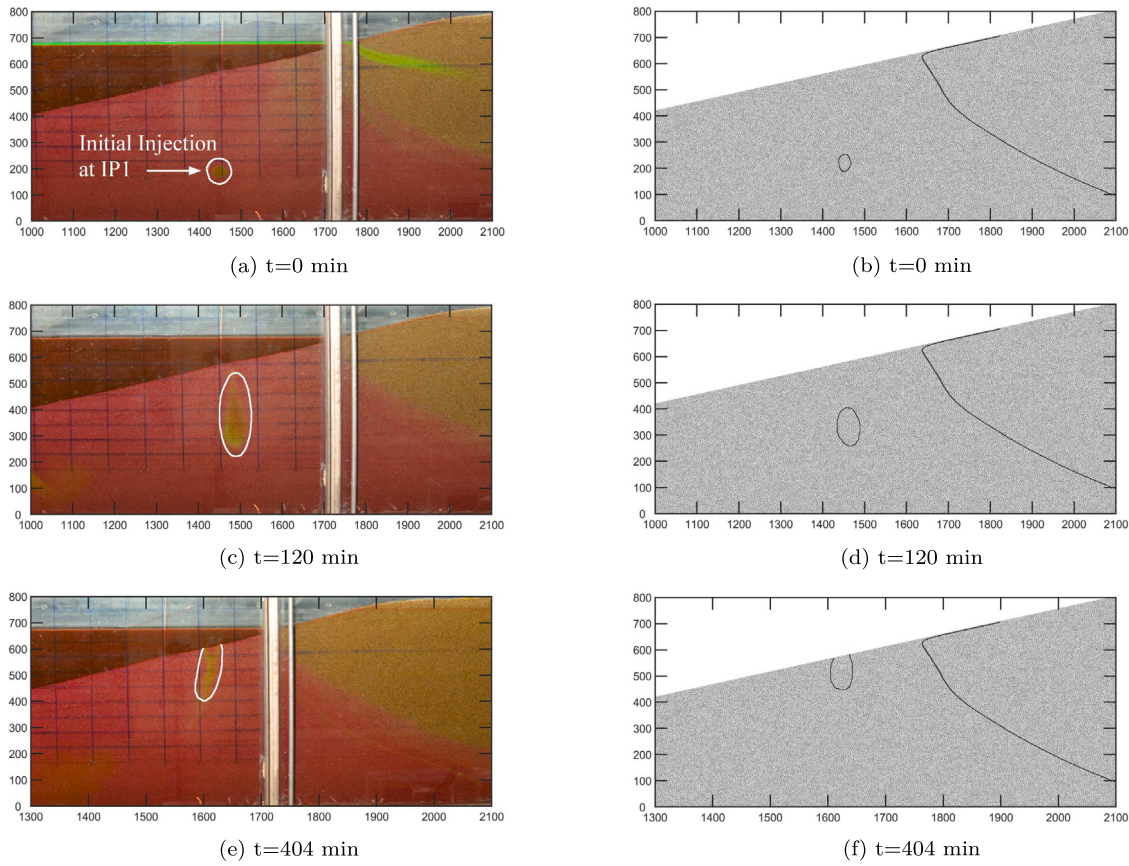


Fig. 8. The results of the laboratory experiment, which show the point source movement with time.

Numerically simulated pressure head (**Fig. 12**) and experimental hydraulic head values were plotted to check the consistency of the obtained results. **Fig. 13** shows the plot corresponding to homogeneous unconfined porous media configuration.

The plot shows match of the results within 2 cm band for four pressure probes (PS1, PS2, PS3, PS5). The cluster outliers (PS4 & PS6) are clearly visible from the plot. Those outlier zones are considered to be cluster of pressure transducer locations. PS4 (**Fig. 1(a)**) is located just below the junction point between sloping porous zone and water level in non-porous zone. Density variation is the possible reason for this discrepancy as water moves out from the freshwater zone (**Fig. 9**) through the junction point. Discrepancy in cluster PS6 may be attributed to right boundary effect (**Fig. 1(a)**). Freshwater flux was provided through right boundary at a constant rate. During the experiment a marginal rise of water level was observed at the right boundary. This leads to overestimation of pore water pressure near boundary.

The transient pore water pressure data provides valuable information for estimation of hydraulic conductivity in density variant flows. However, limited number of studies [58] are available on experimental determination of pore water pressure.

Further the consistency check was performed for configuration with low-permeability strata (**Fig. 14**). The plot shows match of the results within 2 cm band for four pressure probes (PS1, PS2, PS4, PS6) placed below the low-permeability layer. The cluster outliers (PS3 & PS5) are clearly visible from the plot. PS3 was placed near to right boundary above the low permeable layer (Figure S3). Variation in head value may attribute to freshwater flux from the right boundary. PS5 (**Fig. 1(b)** & Figure S3) was placed at the middle portion in unconfined zone above the low permeable layer. Variation in compaction level in unconfined zone is the possible reason for this variation.

Density dependent flows are characterized by the stability of fluid interfaces. It is evident that the fluid interface has irregular boundaries (**Fig. 3**). The SWI moves at a faster rate in the vertical direction compared to the numerical simulation. It was due to the combined effect of hydraulic conductivity, longitudinal dispersivity and transverse dispersivity. Rayleigh number and Peclet number were utilized to characterize the density dependent flow through porous media. A dimensional analysis was performed for identification of the pertinent variables that dictate the stability of fluid interface. List [59] analyzed the stability for a density-stratified horizontal flow in an infinite saturated homogeneous porous medium. Occurrence of instabilities may be related to two Rayleigh numbers [60] as given below

$$R_a^*|_L = \frac{kg\Delta\rho L}{\epsilon\mu D_L}, \quad (2)$$

$$R_a^*|_T = \frac{kg\Delta\rho H}{\epsilon\mu D_T}, \quad (3)$$

$$D_L = V_m \alpha_L, \quad (4)$$

$$D_T = V_n \alpha_T. \quad (5)$$

Where k is the permeability of the porous medium, g is the acceleration due to gravity, $\Delta\rho$ is the density difference between the two fluids, L is the characteristic length, μ is the dynamic viscosity of the fluid, D_L is the longitudinal dispersion coefficient, D_T is the transverse dispersion coefficient and H is the width of the medium. The value of R_a^* value was around 50000 for our experiments. It was concluded in [61] that the transition from stable to unstable plume occurs between $R_a^* = 150$ to 250 or 750 depending on D_T calculation procedure. According to these criteria, the flow and transport experiments appear to be stable. The numerical modeling and generation of the instabilities are beyond the scope of this paper. In our modeling, neither artificial

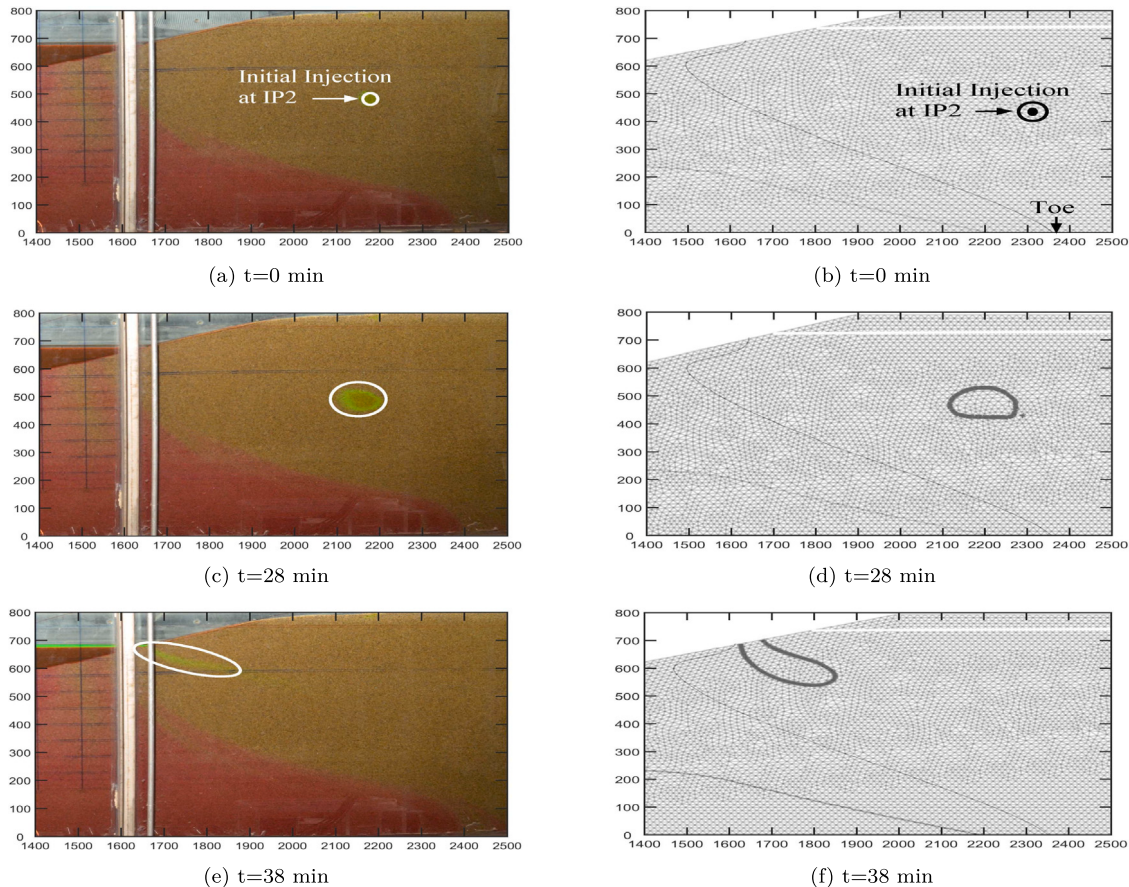


Fig. 9. Movement of tracer plume at point source during experiment showing the freshwater flux with time.

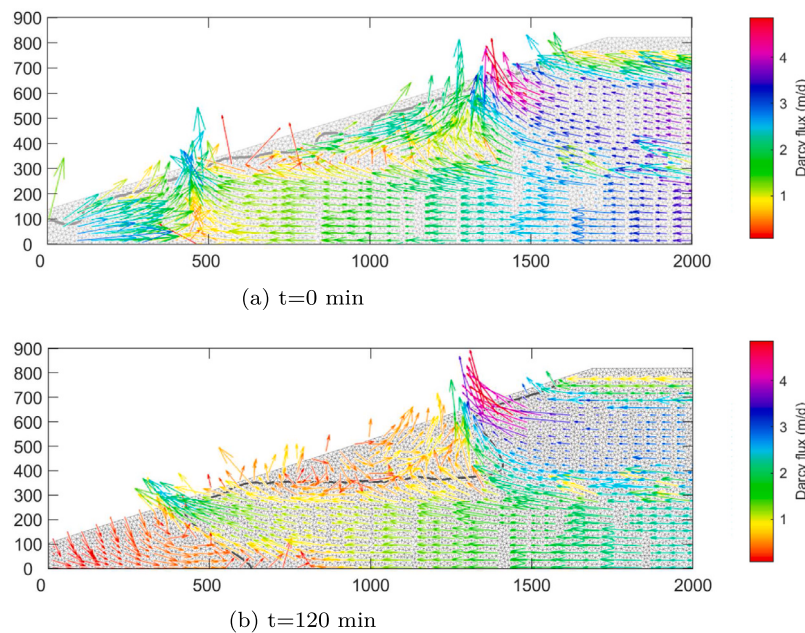


Fig. 10. Fluid-flow patterns and mass transport in low-permeability strata. The vectors represent the Darcy flux of fluid flow with time.

disturbances nor numerical errors were introduced. Therefore, such instabilities are not present in the numerical results. It is evident that more experimental and theoretical studies are needed to investigate the behavior of dense plumes in general.

6. Summary and conclusions

The present study provides variable density flow phenomena observed in laboratory experiments as benchmark test cases. Comparison

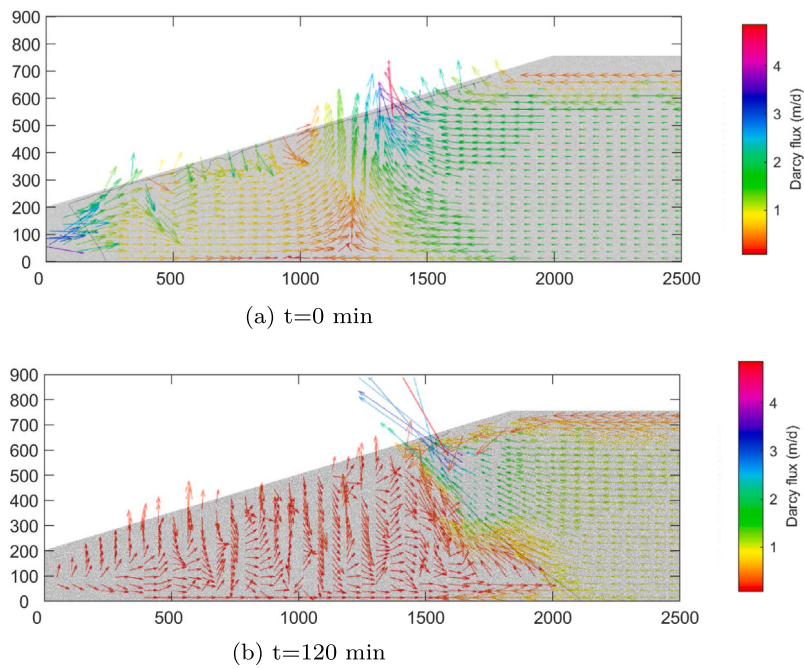


Fig. 11. Fluid-flow patterns and mass transport in homogeneous configuration. The vectors represent the Darcy flux of fluid flow with time.

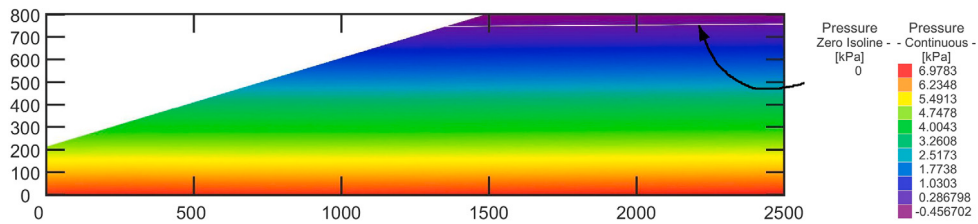


Fig. 12. Physical base simulated Pressure distribution.

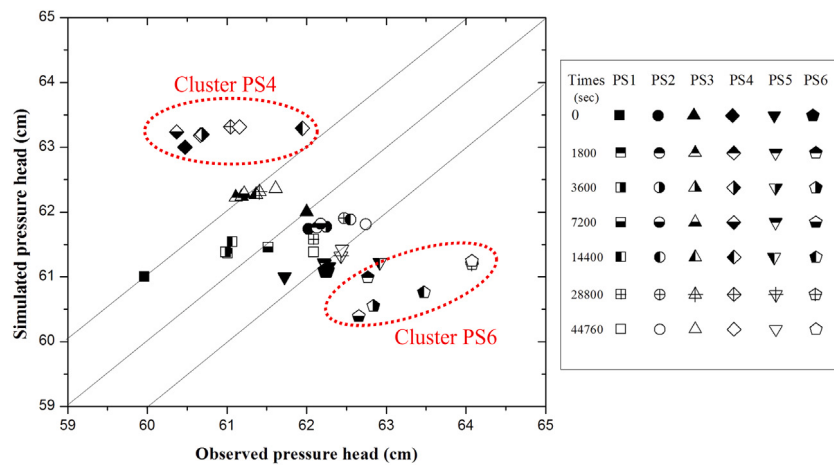


Fig. 13. Comparison between observed and simulated pressure head data with time in homogeneous configuration.

between experiments and the numerical simulation includes quantification of variable density circulation and flow patterns. A two-dimensional sand box model was utilized to physically simulate saltwater intrusion phenomenon such as initial saltwater fingering, effect of low permeability strata and circulation. Experiments were conducted in the glass test section with dye and clean sand (as the aquifer material).

Data were acquired in the form of color images and pore water pressure through pressure transducers. Overall study can be summarized as following:

- (i) Concentration (Rhodamine dye plume) contour maps were obtained from the processed images. SWI movement pattern can be quantified through image analysis.

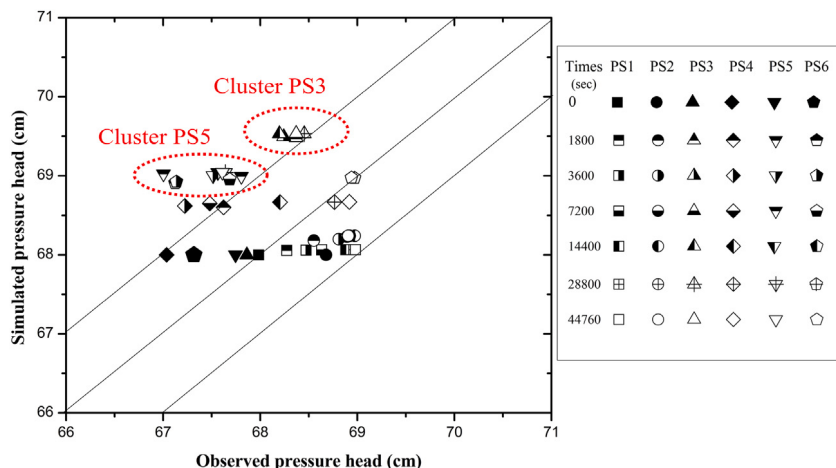


Fig. 14. Comparison between observed and simulated pressure head in low permeability layer configuration.

- (ii) Pore water pressure captured through pressure transducers effectively captures the time evolution of density front over space. Importance of freshwater flux is evident from these experiments. Direct quantification of inward movement of saltwater is possible with pore water pressure measurement.
- (iii) The experimental results show qualitative match with the results obtained through numerical simulations. However, the numerical results over-estimates front movement. Darcy's law grossly averages the momentum effect. Thus fingering effect in porous media was not captured in the present numerical simulations.
- (iv) The present study suggests a three step combined methodology to quantify the variable-density flow patterns. The pore water pressure measurements are acceptable at laboratory scale. However, the relative error will sufficiently reduce during field scale applications.

Future studies should address submarine groundwater discharge calculation; nutrient flow in river-water and fresh groundwater systems; identification of ocean circulation induced patterns.

CRediT authorship contribution statement

Chitaranjan Dalai: Writing - original draft, Conceptualization, Experimental investigation, Simulation & validation. **Selva Balaji Munusamy:** Experimental investigation, Writing - review & editing. **Anirban Dhar:** Conceptualization, Methodology, Writing - review & editing.

Declaration of competing interest

The authors declare that they have no known competing financial interests or personal relationships that could have appeared to influence the work reported in this paper.

Acknowledgments

This research was supported by Department of Science and Technology (DST), Government of India (Grant Number: SB/FTP/ETA-0356/2013). Authors would like to acknowledge D. D. Engineering Industries, Kolkata.

Appendix A. Supplementary data

The Supporting Information documents are linked to this manuscript. The materials consist of data provided by the author that are presented to ensure clarity for readers. Additional details of the figures are provided in the Supporting Materials.

Figures S1: Schematic representation of overall Methodology. Figures S2: Photograph details test-section of experimental sandbox model setup. Figures S3: Boundary conditions for the numerical simulations for Low-permeability configuration.

Supplementary material related to this article can be found online at <https://doi.org/10.1016/j.flowmeasinst.2020.101794>.

References

- [1] M. Simpson, T. Clement, Theoretical analysis of the worthiness of Henry and Elder problems as benchmarks of density-dependent groundwater flow models, *Adv. Water Resour.* 26 (1) (2003) 17–31.
- [2] W.R. Souza, C.I. Voss, Analysis of an anisotropic coastal aquifer system using variable-density flow and solute transport simulation, *J. Hydrol.* 92 (1–2) (1987) 17–41.
- [3] K.-Y. Kim, C.-M. Chon, K.-H. Park, A simple method for locating the fresh water-salt water interface using pressure data, *Groundwater* 45 (6) (2007) 723–728.
- [4] D. MacAllister, M. Jackson, A. Butler, J. Vinogradov, Remote detection of saline intrusion in a coastal aquifer using borehole measurements of self-potential, *Water Resour. Res.* 54 (3) (2018) 1669–1687.
- [5] R.J. Schotting, H. Moser, S.M. Hassanzadeh, High-concentration-gradient dispersion in porous media: experiments, analysis and approximations, *Model. Anal. Simul. (R 9734)* (1997).
- [6] S. Watson, D. Barry, R. Schotting, S. Hassanzadeh, Validation of classical density-dependent solute transport theory for stable, high-concentration-gradient brine displacements in coarse and medium sands, *Adv. Water Resour.* 25 (6) (2002) 611–635.
- [7] C.-Y. Jiao, H. Hötzl, An experimental study of miscible displacements in porous media with variation of fluid density and viscosity, *Transp. Porous Media* 54 (2) (2004) 125–144.
- [8] T.C. Flowers, J.R. Hunt, Viscous and gravitational contributions to mixing during vertical brine transport in water-saturated porous media, *Water Resour. Res.* 43 (1) (2007).
- [9] Q. Zhang, R.E. Volker, D.A. Lockington, Experimental investigation of contaminant transport in coastal groundwater, *Adv. Environ. Res.* 6 (3) (2002) 229–237.
- [10] R.R. Goswami, T. Clement, Laboratory-scale investigation of saltwater intrusion dynamics, *Water Resour. Res.* 43 (4) (2007).
- [11] M. Konz, P. Ackerer, E. Meier, P. Huggenberger, E. Zechner, D. Gechter, On the measurement of solute concentrations in 2-D flow tank experiments, *Hydrolog. Earth Syst. Sci. Discuss.* 12 (3) (2008) 727–738.
- [12] R.A. Schincariol, F.W. Schwartz, An experimental investigation of variable density flow and mixing in homogeneous and heterogeneous media, *Water Resour. Res.* 26 (10) (1990) 2317–2329.
- [13] M. Konz, A. Younes, P. Ackerer, M. Fahs, P. Huggenberger, E. Zechner, Variable-density flow in heterogeneous porous media—Laboratory experiments and numerical simulations, *J. Contam. Hydrol.* 108 (3–4) (2009) 168–175.
- [14] M. Konz, P. Ackerer, A. Younes, P. Huggenberger, E. Zechner, Two-dimensional stable-layered laboratory-scale experiments for testing density-coupled flow models, *Water Resour. Res.* 45 (2) (2009).
- [15] S.W. Chang, T.P. Clement, Laboratory and numerical investigation of transport processes occurring above and within a saltwater wedge, *J. Contam. Hydrol.* 147 (2013) 14–24.

- [16] E.J. Dose, L. Stoeckl, G.J. Houben, H. Vacher, S. Vassolo, J. Dietrich, T. Himmelsbach, Experiments and modeling of freshwater lenses in layered aquifers: steady state interface geometry, *J. Hydrol.* 509 (2014) 621–630.
- [17] S.S. Mehdizadeh, A.D. Werner, F. Vafaei, S. Badaruddin, Vertical leakage in sharp-interface seawater intrusion models of layered coastal aquifers, *J. Hydrol.* 519 (2014) 1097–1107.
- [18] A.D. Werner, M. Bakker, V.E. Post, A. Vandebosch, C. Lu, B. Ataie-Ashtiani, C.T. Simmons, D.A. Barry, Seawater intrusion processes, investigation and management: recent advances and future challenges, *Adv. Water Resour.* 51 (2013) 3–26.
- [19] N. Shokri, M.M. Namin, J. Farhoudi, A three-dimensional non-hydrostatic coupled model for free surface–Subsurface variable–Density flows, *J. Contam. Hydrol.* 216 (2018) 38–49.
- [20] A. Abudawia, A. Mourad, J. Rodrigues, C. Rosier, A finite element method for a seawater intrusion problem in unconfined aquifers, *Appl. Numer. Math.* 127 (2018) 349–369.
- [21] B. Lèye, J. Koko, S. Kane, M. Sy, Numerical simulation of saltwater intrusion in coastal aquifers with anisotropic mesh adaptation, *Math. Comput. Simulation* 154 (2018) 1–18.
- [22] N. Shokri, M. Montazeri Namin, J. Farhoudi, An implicit 2D hydrodynamic numerical model for free surface–subsurface coupled flow problems, *Internat. J. Numer. Methods Fluids* 87 (7) (2018) 343–357.
- [23] I. Oz, E. Shalev, Y. Yechiel, H. Gvirtzman, Saltwater circulation patterns within the freshwater–saltwater interface in coastal aquifers: Laboratory experiments and numerical modeling, *J. Hydrol.* 530 (2015) 734–741.
- [24] M. Dentz, D. Tartakovsky, E. Abarca, A. Guadagnini, X. Sanchez-Vila, J. Carrera, Variable-density flow in porous media, *J. Fluid Mech.* 561 (2006) 209–235.
- [25] O. Manickam, G. Homsy, Fingering instabilities in vertical miscible displacement flows in porous media, *J. Fluid Mech.* 288 (1995) 75–102.
- [26] R. Wooding, S.W. Tyler, I. White, Convection in groundwater below an evaporating salt lake: 1. Onset of instability, *Water Resour. Res.* 33 (6) (1997) 1199–1217.
- [27] C.T. Simmons, T.R. Fenstemaker, J.M. Sharp Jr., Variable-density groundwater flow and solute transport in heterogeneous porous media: approaches, resolutions and future challenges, *J. Contam. Hydrol.* 52 (1–4) (2001) 245–275.
- [28] H.-J. Diersch, O. Kolditz, Variable-density flow and transport in porous media: approaches and challenges, *Adv. Water Resour.* 25 (8–12) (2002) 899–944.
- [29] R.A. Schincariol, F.W. Schwartz, C.A. Mendoza, On the generation of instabilities in variable density flow, *Water Resour. Res.* 30 (4) (1994) 913–927.
- [30] C.-H. Lee, R.T.-S. Cheng, On seawater encroachment in coastal aquifers, *Water Resour. Res.* 10 (5) (1974) 1039–1043.
- [31] R. Volker, K. Rushton, An assessment of the importance of some parameters for seawater intrusion in aquifers and a comparison of dispersive and sharp-interface modelling approaches, *J. Hydrol.* 56 (3–4) (1982) 239–250.
- [32] M.J. Simpson, T.P. Clement, Improving the worthiness of the henry problem as a benchmark for density-dependent groundwater flow models, *Water Resour. Res.* 40 (1) (2004).
- [33] E. Mehner, A.A. Jennings, The effect of salinity-dependent hydraulic conductivity on saltwater intrusion episodes, *J. Hydrol.* 80 (3–4) (1985) 283–297.
- [34] C.T. Simmons, K.A. Narayan, Mixed convection processes below a saline disposal basin, *J. Hydrol.* 194 (1–4) (1997) 263–285.
- [35] C. Lu, Y. Chen, C. Zhang, J. Luo, Steady-state freshwater-seawater mixing zone in stratified coastal aquifers, *J. Hydrol.* 505 (2013) 24–34.
- [36] A. Abdoulhalik, A.A. Ahmed, How does layered heterogeneity affect the ability of subsurface dams to clean up coastal aquifers contaminated with seawater intrusion? *J. Hydrol.* 553 (2017) 708–721.
- [37] A. Abdoulhalik, A.A. Ahmed, The effectiveness of cutoff walls to control saltwater intrusion in multi-layered coastal aquifers: Experimental and numerical study, *J. Environ. Manag.* 199 (2017) 62–73.
- [38] H. Diersch, FEFLOW finite element subsurface flow and transport simulation system reference manual, WASY inst. for water resour, Plann. Syst. Res., Berlin (2002).
- [39] B. Ataie-Ashtiani, R. Volker, D. Lockington, Numerical and experimental study of seepage in unconfined aquifers with a periodic boundary condition, *J. Hydrol.* 222 (1–4) (1999) 165–184.
- [40] M. Oostrom, J. Hayworth, J. Dane, O. Güven, Behavior of dense aqueous phase leachate plumes in homogeneous porous media, *Water Resour. Res.* 28 (8) (1992) 2123–2134.
- [41] C.T. Simmons, M. Pierini, J. Hutson, Laboratory investigation of variable-density flow and solute transport in unsaturated–saturated porous media, *Transp. Porous Media* 47 (2) (2002) 215–244.
- [42] A.D. Werner, D. Jakovovic, C.T. Simmons, Experimental observations of saltwater up-coning, *J. Hydrol.* 373 (1–2) (2009) 230–241.
- [43] L. Shi, L. Cui, N. Park, P.S. Huyakorn, Applicability of a sharp-interface model for estimating steady-state salinity at pumping wells—validation against sand tank experiments, *J. Contam. Hydrol.* 124 (1–4) (2011) 35–42.
- [44] H.-J.G. Diersch, FEFLOW: Finite Element Modeling of Flow, Mass and Heat Transport in Porous and Fractured Media, Springer Science & Business Media, 2013.
- [45] E. Abarca, T.P. Clement, A novel approach for characterizing the mixing zone of a saltwater wedge, *Geophys. Res. Lett.* 36 (6) (2009).
- [46] R.A. Freeze, J.A. Cherry, A. 1979. Groundwater, vol. 604, Prentice-Hall, Inc Englewood cliffs, New Jersey, 1974, pp. 215–227.
- [47] F. Catania, M. Massabo, M. Valle, G. Bracco, O. Paladino, Assessment of quantitative imaging of contaminant distributions in porous media, *Exp. Fluids* 44 (1) (2008) 167–177.
- [48] S. Jaeger, M. Ehn, C. Eberhardt, M. Rolle, P. Grathwohl, G. Gauglitz, CCD camera image analysis for mapping solute concentrations in saturated porous media, *Anal. Bioanal. Chem.* 395 (6) (2009) 1867.
- [49] P.M. Oates, C.F. Harvey, A colorimetric reaction to quantify fluid mixing, *Exp. Fluids* 41 (5) (2006) 673–683.
- [50] Å. Olsson, P. Grathwohl, Transverse dispersion of non-reactive tracers in porous media: a new nonlinear relationship to predict dispersion coefficients, *J. Contam. Hydrol.* 92 (3–4) (2007) 149–161.
- [51] C.J. Werth, C. Zhang, M.L. Brusseau, M. Oostrom, T. Baumann, A review of non-invasive imaging methods and applications in contaminant hydrogeology research, *J. Contam. Hydrol.* 113 (1–4) (2010) 1–24.
- [52] B. Zinn, L.C. Meigs, C.F. Harvey, R. Haggerty, W.J. Peplinski, C.F. von Schwerin, Experimental visualization of solute transport and mass transfer processes in two-dimensional conductivity fields with connected regions of high conductivity, *Environ. Sci. Technol.* 38 (14) (2004) 3916–3926.
- [53] G. Robinson, G. Hamill, A.A. Ahmed, Automated image analysis for experimental investigations of salt water intrusion in coastal aquifers, *J. Hydrol.* 530 (2015) 350–360.
- [54] P. Aeby, J. Forrer, H. Flühler, C. Steinmeier, Image analysis for determination of dye tracer concentrations in sand columns, *Soil Sci. Am. J.* 61 (1) (1997) 33–35.
- [55] J.A. Richards, J. Richards, Remote Sensing Digital Image Analysis, vol. 3, Springer, 1999.
- [56] D.A. Sabatini, T.A. Austin, Characteristics of rhodamine WT and fluorescein as adsorbing ground-water tracers, *Groundwater* 29 (3) (1991) 341–349.
- [57] S. Yoon, J.R. Williams, R. Juanes, P.K. Kang, Maximizing the value of pressure data in saline aquifer characterization, *Adv. Water Resour.* 109 (2017) 14–28.
- [58] P.K. Kang, J. Lee, X. Fu, S. Lee, P.K. Kitanidis, R. Juanes, Improved characterization of heterogeneous permeability in saline aquifers from transient pressure data during freshwater injection, *Water Resour. Res.* 53 (5) (2017) 4444–4458.
- [59] E.J. List, The Stability and Mixing of a Density-Stratified Horizontal Flow in a Saturated Porous Medium (Ph.D. thesis), California Institute of Technology, 1965.
- [60] R. Wooding, Convection in a saturated porous medium at large Rayleigh number or Peclet number, *J. Fluid Mech.* 15 (4) (1963) 527–544.
- [61] M. Oostrom, J. Dane, O. Güven, J. Hayworth, W. Hill, Concentration measurements in dense leachate plumes using a gamma radiation system, in: Symposium on Ground Water, ASCE, 1991, pp. 287–292.